Molecular Mechanisms of Interaction of Rabbit CAP18 with Outer Membranes of Gram-Negative Bacteria†

Thomas Gutsmann,‡ James W. Larrick,§ Ulrich Seydel,‡ and Andre Wiese*,‡

Department of Immunochemistry and Biochemical Microbiology, Center for Medicine and Biosciences, Research Center Borstel, Parkallee 10, D-23845 Borstel, Germany, and Palo Alto Institute of Molecular Medicine, 2462 Wyandotte Street, Mountain View, California 94043

Received March 19, 1999; Revised Manuscript Received July 13, 1999

ABSTRACT: The mechanism of interaction of the cationic antimicrobial protein (18 kDa), CAP18, with the outer membrane of Gram-negative bacteria was investigated applying transmission electron microscopy and voltage-clamp techniques on artificial planar bilayer membranes. Electron micrographs of bacterial cells exposed to CAP18 showed damage to the outer membrane of the sensitive *Escherichia coli* strains F515 and ATCC 11775, whereas the membrane of the resistant *Proteus mirabilis* strain R45 remained intact. Electrical measurements on various planar asymmetric bilayer membranes, one side consisting of a phospholipid mixture and the other of different phospholipids or of lipopolysaccharide (reconstitution model of the outer membrane), yielded information about the influence of CAP18 on membrane integrity. Addition of CAP18 to the side with the varying lipid composition led to lipid-specific adsorption of CAP18 and subsequent induction of current fluctuations due to the formation of transient membrane lesions at a lipid-specific clamp voltage. We propose that the applied clamp voltage leads to reorientation of CAP18 molecules adsorbed to the bilayer into an active transmembrane configuration, allowing the formation of lesions by multimeric clustering.

Neutrophilic granulocytes are essential in the primary defense against intruding microorganisms. They contain intracellular granules as a major site of storage of antimicrobial proteins and peptides which are liberated into the phagocytic vacuoles during phagocytosis (*1*). One of these substances is the 18 kDa cationic antibacterial protein (CAP18)[1] which was originally isolated from rabbit granulocytes using as an assay the agglutination of lipopolysaccharide (LPS)-coated erythrocytes (*2*). Interestingly, the human plasma concentration of CAP18 (1.18 μg/mL) is several-fold higher than those of other neutrophil-specific granule proteins (*3*).

CAP18 exhibits LPS-binding, LPS-neutralizing, antibacterial, and anticoagulant activities (*4*). These properties are shared with other cationic antibacterial peptides/proteins such as the antibiotic polymyxin B, defensins, and the bactericidal/permeability-increasing protein (BPI). There are, however, no sequence homologies between these peptides. CAP18 consists of 142 amino acids with the bioactivity found in the C-terminal fragment of 37 amino acids ($CAP18_{106-142}$) (*5*). This C-terminal fragment carries two negative and 15 positive amino acids and has a high-affinity binding site for heparin (*6*). In contrast, the N-terminal part of CAP18 is nearly uncharged (17 negative and 15 positive amino acids). Ogata et al. (*7*) showed that heparin inhibited the ability of $CAP18_{106-138}$ to suppress LPS-induced TNF production in whole blood. Thus, the active part of CAP18 is highly cationic, and an electrostatic interaction with the negative charges of the cell wall of sensitive bacteria is likely.

The secondary structure of $CAP18_{106-137}$, determined by Chen et al. (*8*) with nuclear magnetic resonance measurements, was found to be a complete and very rigid helix. The solution structure of this fragment exists in at least three different helix conformations depending on the lipid A concentration. The importance of the secondary structure and amphiphilicity of CAP18 for the interaction with the bacterial membrane was noted by Tossi et al. (*9*). These authors showed that disruption of the α-helix of $CAP18_{106-125}$ by substitution with various amino acids (e.g., proline) eliminated antibacterial activity and that certain changes in the

† This work was financially supported by the Deutsche Forschungsgemeinschaft (Grant SFB 470, Project B5) and the Federal Ministry of Eduction, Science, Research, and Technology (BMBF, Grant 01 KI 9851, Project A6).

* To whom correspondence should be addressed. Phone: +49 (0) 4537 188-291. Fax: +49 (0) 4537 188-632. E-mail awiese@fz-borstel.de.

‡ Research Center Borstel.

§ Palo Alto Institute of Molecular Medicine.

[1] Abbreviations: CAP18, 18 kDa cationic antibacterial protein; LPS, lipopolysaccharide(s); F515 LPS, LPS of *Escherichia coli* Re mutant strain F515; R595 LPS, LPS of *Salmonella enterica* sv. Minnesota Re mutant strain R595; R45 LPS, LPS of *Proteus mirabilis* Re mutant strain R45; MDO, membrane-derived oligosaccharide; PG, phosphatidylglycerol; PE, phosphatidylethanolamine; DPG, diphosphatidylglycerol; PL, phospholipid mixture of PE, PG, and DPG in a molar ratio of 81/17/2; DPhyPC, diphytanoylphosphatidylcholine; TEM, transmission electron microscopy; TNF, tumor necrosis factor; L-Ara*p*4N, 4-amino-4-deoxy-L-*arabino*-pentopyranose; V_{min}, minimal clamp voltage; c_{min}, minimal concentration; PMB, polymyxin B; PMBN, polymyxin B nonapeptide; A_M, area of the membrane; C_M, capacitance of the membrane; I, current; U, clamp voltage; U_{GC}, Gouy−Chapman potential; U_D, dipole potential; U_B, Born potential; $\Delta\Phi$, innermembrane potential difference.

10.1021/bi990643v CCC: $18.00
Published on Web 09/23/1999

amphiphilicity have a greater effect on the activity than the reduction of the positive charges.

Gram-negative bacteria [50% inhibitory concentration of 20−100 nM (0.4−2 μg/mL)] such as *Escherichia coli*, *Salmonella minnesota*, and *Salmonella typhimurium* and Gram-positive bacteria [50% inhibitory concentration of 130−200 nM (2.3−3.6 μg/mL)] such as *Streptococcus pneumoniae* and *Staphylococcus aureus* are known to be sensitive to the antimicrobial action of CAP18. There is, however, no activity of CAP18 against the Gram-negative strain of *Proteus mirabilis*, fungi, and multiple-drug resistant strains of *Mycobacterium avium* and *Mycobacterium tuberculosis* (*10*). A dependence of $CAP18_{106-137}$ activity on the salt concentration of K^+ (50−250 mM) and Mg^{2+} (1−10 mM) was not observed (*11*).

The cell envelope of Gram-negative bacteria consists of the cytoplasmic membrane, the peptidoglycan layer, and an additional barrier, the outer membrane which is strictly asymmetric with respect to its lipid composition. This outer membrane is the primary target of CAP18 and other antibacterial peptides and proteins. Whereas the inner leaflet of this membrane contains only phospholipids, the outer leaflet is composed of LPS. LPS consists of an oligo- or polysaccharide portion which is covalently linked to a lipid component, termed lipid A, which anchors the molecule in the membrane (*12*).

Depending on the species and/or strain from which the LPS was obtained, each LPS molecule carries different numbers of negative charges such as carboxyl or phosphoryl groups. In the paper presented here, LPS with the shortest sugar moieties was used to reconstitute planar membranes, i.e., deep rough mutant LPS (Re LPS) carrying two Kdo units at the lipid A. For the TEM studies, we also used the wild-type *E. coli* ATCC 11775 strain.

Nearly solvent-free and asymmetric planar bilayer membranes were formed according to the method introduced by Montal and Mueller (*13*) to characterize the electrical interaction of CAP18 with the outer membrane. Using these model membranes, we have studied the influence of the lipid matrix, in particular that of the net charges of the composing lipids. One leaflet, representing the bacterial inner leaflet, consisted of a phospholipid mixture termed PL, and the other of either LPS from deep rough mutant strains of CAP18-sensitive (*E. coli* F515 and *S. minnesota* R595) or resistant (*P. mirabilis* R45) bacteria or the electrically neutral diphytanoylphosphatidylcholine (DPhyPC). This system of reconstituted membranes allowed us to obtain information about CAP18-induced changes in the electrical properties of the lipid bilayer such as membrane capacitance, inner-membrane potential difference (determined from current−voltage curves of K^+-carrier-doped membranes), and membrane conductivity.

On the basis of our results, we propose the following model of the action of CAP18 on the reconstituted outer membrane of Gram-negative bacteria. CAP18 intercalates only into lipid matrixes with a negative surface charge density. The binding and intercalation of CAP18 results in significant changes in membrane capacitance, innermembrane potential, and membrane current, influencing membrane permeability for hydrophobic molecules which subsequently causes membrane rupture.

Differences between sensitive and resistant bacteria seen in the TEM pictures of morphological changes of the outer membrane and in electrical effects in planar membranes induced by CAP18 can be explained by this model.

EXPERIMENTAL PROCEDURES

Lipids and Other Chemicals. For the formation of asymmetric LPS/PL membranes, deep rough mutant LPS from *E. coli* strain F515 (F515 LPS), *Salmonella enterica* sv. Minnesota strain R595 (R595 LPS), and *P. mirabilis* strain R45 (R45 LPS) (chemical structures from refs *12* and *14*−*17*) were used. LPS were extracted by the phenol/chloroform/petroleum ether method (*18*), purified, lyophilized, and transformed into the triethylamine salt form. The amounts of nonstoichiometric substitution by fatty acids, L-Ara*p*4N, and phosphoethanolamine (P-Etn) were analyzed by MALDI-TOF mass spectrometry. Thus, in the R595 LPS, the 16:0 fatty acid linked to the amide-linked 3-OH-14:0 in position 2 of the reducing glucosamine was present only at a level of 30%, and L-Ara*p*4N linked to the 4′-phosphate at a level of 65%. In R45 LPS, approximately 50% of the phosphates linked to the 4′-phosphate of lipid A and 50% of the first Kdo were substituted with L-Ara*p*4N.

Phosphatidylethanolamine (PE) from bovine brain (type I), phosphatidylglycerol (PG) from egg yolk lecithin (sodium salt), and diphosphatidylglycerol (DPG) from bovine heart (sodium salt) were from Sigma (Deisenhofen, Germany), and diphytanoylphosphatidylcholine (DPhyPC) was from Avanti Polar Lipids (Alabaster, AL). All phospholipids were used without further purification.

Heparin, purchased from Braun (Melsungen, Germany), had a concentration of 25 000 IU/5 mL (≅2 mmol/L) in NaCl.

The K^+-carrier nonactin was obtained from Sigma (Deisenhofen, Germany).

Proteins. Synthetic rabbit CAP18 was prepared by Merrifield synthesis as previously described (*5*) and stored in 0.01% acetic acid.

Transmission Electron Microscopy (TEM). TEM was employed to confirm morphological changes of the bacterial cell. Log-phase *E. coli* ATCC 11775, *E. coli* F515, and *P. mirabilis* R45 cells (approximately 10^8 cells/mL) incubated for 30 min in various concentrations of CAP18 were centrifuged at 7000*g* for 20 min, prefixed in 2% w/v agar, postfixed in 2% w/v osmium tetroxide for 1 h, contrasted in 2% w/v uranyl acetate for 1 h, and dehydrated in ethanol. Pellets were embedded in epon-prophyloxid and polymerized for 12 h at 60 °C. Sections were stained with lead citrate and examined with a Zeiss EM910 transmission electron microscope at 80 kV.

Preparation of Planar Bilayers and Electrical Measurements. Planar bilayers according to the Montal−Mueller technique (*13*) were prepared as described previously (*19*). Briefly, asymmetric bilayers were formed by opposing two lipid monolayers prepared on aqueous subphases (bathing solutions) from chloroformic solutions of the lipids at a small aperture (typically 150 μm diameter) in a thin Teflon septum (12.5 μm thick). The essential step in bilayer reconstitution is the formation of lipid monolayers. This step requires a chloroform or chloroform/methanol solubility and a sufficiently high hydrophobicity of the lipids. This requirement is not fulfilled by wild-type LPS.

The apparatus for membrane formation consisted of two Teflon compartments each with a 1.5 mL volume. Prior to membrane formation, the septum was pretreated with a hexane/hexadecane mixture (20/1 v/v). For the formation of bilayer membranes, natural phospholipids and DPhyPC were dissolved in chloroform (2.5 mg/mL) and LPS (2.5 mg/mL) in chloroform/methanol (10/1 v/v) by heating to 95 °C for 2 min. The PL leaflet of asymmetric LPS/PL membranes consisted of a mixture of PE, PG, and DPG in a molar ratio of 81/17/2, resembling the phospholipid composition of the inner leaflet of the outer membrane of *S. typhimurium* (*20*) being composed of the same constituents as that of the other strains that were used (*21*).

For electrical measurements, planar membranes were voltage-clamped via a pair of Ag/AgCl electrodes (type IVM E255, Advanced Laboratory Research Inc.) connected to the head stage of an L/M-PCA patch clamp amplifier (List-Medical, Darmstadt, Germany). In all cases, the compartment opposite (trans compartment) the one to which the peptide (cis compartment) was added was grounded. Therefore, in comparison to the natural system, a positive clamp voltage represents a membrane which is negative on the inner side. Current was defined as positive when cation flux was directed toward the grounded compartment. Membrane current and clamp voltage were stored using a digital tape recorder (DTR 1202, Biologic, Claix, France). The stored signals were low-pass filtered with a four-pole Bessel filter (Ithaco model 4302, Ithaca, NY), sent to the microcomputer system, and digitized with a PCI-200428W-1 analog input board (Intelligent Instrumentation, Leinfelden-Echterdingen, Germany). For the determination of the single fluctuation amplitudes, the current traces were filtered at a corner frequency of 2.5 kHz and digitized with a sampling frequency of 7 kHz.

Most measurements were performed with a bathing solution consisting of 100 mM KCl and 5 mM $MgCl_2$ at a temperature of 37 °C. To adjust to pH 7, the bathing solutions were buffered with 5 mM HEPES. The specific electrical conductivity of the bathing solutions at 37 °C was 17.2 mS cm^{-1}. In some experiments, the KCl or $MgCl_2$ concentrations were changed as indicated.

At the beginning of each experiment, the correct membrane formation was checked by measuring the membrane current and capacitance. Only membranes with a basic current of less than 2.5 pA at a clamp voltage of ±100 mV and a capacitance of more than 90 pF (diameter of the aperture of 150 μm) were used for the experiments. CAP18 was added in aliquots of 15 μL up to the respective final concentration to the compartment opposite the PL side of the bilayer.

Membrane Capacitance. The determination of the membrane capacitance yields information about the area, thickness, and composition of the bilayer. The capacitance C_M of the hydrophobic core of the bilayer is

$$C_M = \epsilon_0 \epsilon_r \frac{A_M}{d} \quad (1)$$

where $\epsilon_0 = 8.854 \times 10^{-12}$ F/m, ϵ_r is the dielectric coefficient, d is the thickness of the alkyl interior, and A_M is the effective area of the bilayer.

Membrane capacitance can be determined by applying step-like voltage pulses and measuring the resulting transient charging currents (*22*). In our setup, the bit steps of the digital−analog converter (DAC) were used to obtain fast pulses with a very small amplitude (4.9 μV). To increase the accuracy, a voltage ramp consisting of 409 steps was applied and the respective rectified current responses were integrated. This method allowed us to determine the capacitance at a frequency of 1 Hz and a maximum clamp voltage of 1 mV. In this way, we were able to analyze membrane qualities and membrane−protein interactions without influencing the system with other agents such as carriers or with high clamp voltages.

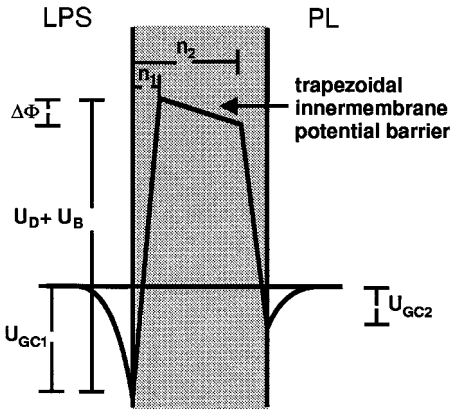

FIGURE 1: Schematic representation of the simplified intrinsic membrane profile for F515 LPS/PL membranes. Negative surface charges induce the Gouy−Chapman potential U_{GC}. The trapezoidal innermembrane potential barrier is caused by the dipole potential (U_D) and the self-energy (Born potential, U_B). $\Delta\Phi$ is the innermembrane potential difference; n_1 and n_2 are positions of the corners of the trapezoidal potential barrier.

Membrane Potential. The intrinsic membrane potential is composed of the surface and the innermembrane potential. The sum of the intrinsic potential and a potential resulting from an externally applied clamp voltage (or from a transmembrane ion gradient) results in the transmembrane potential [Figure 1; adopted from Schoch et al. (*23*) for LPS/PL membranes].

The surface potential is provoked by fixed charges on the membrane surface. The innermembrane potential arises from the dipole potential (U_D) wich is created by dipole moments within the lipid matrix and the interface region of the bilayer and the adsorbed water molecules, and from the Born self-energy (Born potential, U_B) of a charge in the low-dielectric medium of the membrane (*23*).

Extreme asymmetries in charge density as well as in headgroup conformation occur for asymmetric LPS/PL bilayers. Innermembrane potential profiles were derived from I/U curves obtained for K^+-carrier-doped bilayers. For these studies, membranes were prepared as described above. The K^+-carrier nonactin was added to both compartments before membrane preparation at a final concentration of 5×10^{-7} M. The evalution of the I/U curves was carried out according to procedures described previously (*24*). Briefly, the current I as a function of the clamp voltage U is obtained from

$$I_m = K \frac{\Delta\Phi + (n_2 - n_1)U}{n_2 - n_1} \frac{e^{aU} - 1}{e^{a(\Delta\Phi + n_2 U)} - e^{an_1 U}} \quad (2)$$

where $a = (Ze_0)/(kT)$, k is a constant for each membrane, n_1 and n_2 are the relative distances of the edges of the potential

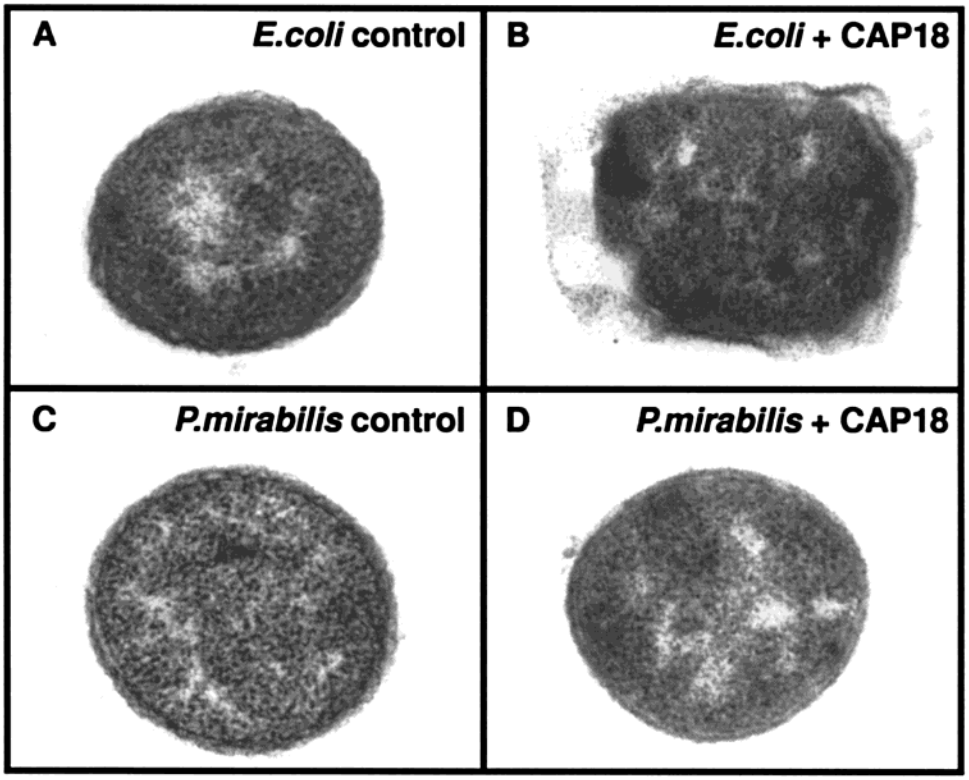

FIGURE 2: Morphological changes of bacterial organisms after CAP18 addition. Typical electron micrographs of single organisms of *E. coli* ATCC 11775 (A and B) and *P. mirabilis* R45 (C and D). (A and C) Controls and (B and D) Organisms after incubation in 280 nM CAP18 for 30 min. The length of one box is 2 μm.

walls for the two leaflets to the membrane surface on the cis side, and $\Delta\Phi$ is the potential difference between these edges (*23*). The three parameters describe the shape of the trapezoidal energy barrier and are determined from the experimental *I*/*U* curves by computer fitting of eq 2.

RESULTS

TEM Studies. To characterize the bactericidal effect of rabbit CAP18, we examined the morphology of bacterial organisms of CAP18-sensitive strains *E. coli* ATCC 11775 and *E. coli* F515 and of the resistant strain *P. mirabilis* R45 after exposure to 110 nM (2 μg/mL) CAP18 for 30 min. Organisms of both *E. coli* strains exhibited an altered membrane morphology, mainly damage to the outer membrane (Figure 2A,B). An exposure to a concentration of 5 μg/mL led to complete damage of most organisms. There was no significant difference in the effects on the wild-type *E. coli* ATCC 11775 and the deep rough mutant *E. coli* F515 strain.

In contrast to these observations, CAP18 induced no changes in the membrane morphology of the CAP18-resistant *P. mirablis* R45 (Figure 2C,D).

Membrane Capacitance. Changes in membrane capacitance after addition of membrane-active agents are indicative of their accumulation or incorporation into the lipid bilayer. Thus, the capacitance changes (height and time course) after the addition of CAP18 yield information about the interaction between the protein and different bilayers.

The addition of 110 nM CAP18 to the negatively charged leaflet of asymmetric membranes led to an increase in membrane capacitance to a maximum of about 125% of the initial value after 3 min, followed by a slow decrease until membrane rupture (Figure 3A,B). The decrease depended significantly on the LPS type that was used: in the case of LPS F515/PL and R595 LPS/PL membranes, minimal capacitance values were lower than that of the undisturbed bilayer, whereas in the case of R45 LPS/PL membranes, the final value was higher (Figure 3B). Similar results were obtained with subphases in the absence of Mg^{2+} ions.

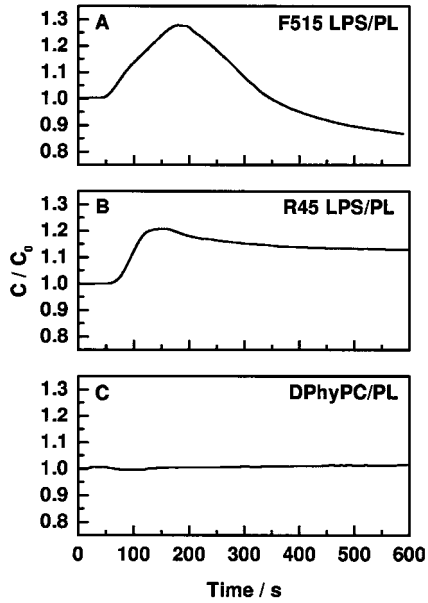

FIGURE 3: CAP18-induced changes in membrane capacitance. Capacitance independence on time after the addition of 110 nM CAP18 to asymmetric bilayers (the side of CAP18 addition is named first): (A) F515 LPS/PL bilayer, (B) R45 LPS/PL, and (C) DPhyPC/PL. The bathing solution was 100 mM KCl, 5 mM $MgCl_2$, and 5 mM HEPES at pH 7 and 37 °C.

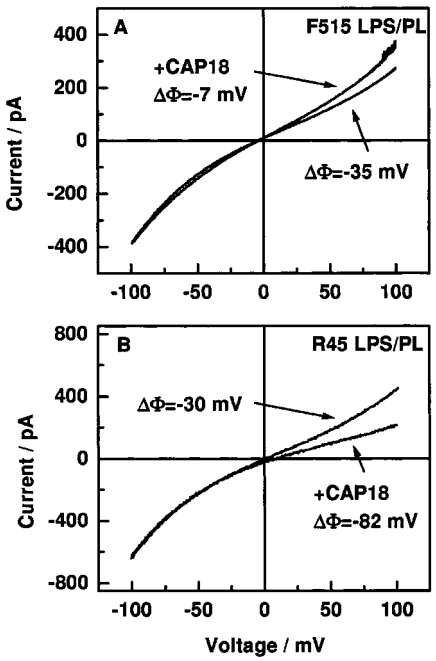

FIGURE 4: CAP18-induced changes in innermembrane potential. *I*/*U* curves of K^+-carrier-mediated ion transport and derived innermembrane potential differences of nonactin-doped asymmetric membranes in the absence and presence of CAP18 (the side of CAP18 addition is named first): (A) F515 LPS/PL bilayer, where $C_{CAP18} = 550$ nM; and (B) R45 LPS/PL, where $C_{CAP18} = 110$ nM. The bathing solution was 100 mM KCl, 5 mM $MgCl_2$, and 5 mM HEPES at pH 7 and 37 °C.

The observed effects were concentration-dependent; the respose increased with increasing CAP18 concentrations up to 110 nM and then reached a plateau (data not shown).

In contrast to the detectable changes in membrane capacitance following CAP18 addition to negatively charged lipids such as F515 LPS, R595 LPS, R45 LPS, and even PL, no changes were observed for the neutral DPhyPC (Figure 3).

Membrane Potential. The determination of the intrinsic membrane potential—a combination of surface potential, dipole potential, and innermembrane potential difference—provides information about the interaction of externally applied compounds, in particular when these substances carry electric charges. The induced changes in the transmembrane potential may influence the membrane permeability and with that the sensitivity of the organisms to antibiotics. Information about innermembrane potential changes was derived from *I*/*U* curves of K^+-carrier-doped planar membranes in the absence and presence of CAP18.

The *I*/*U* curves for asymmetric F515 LPS/PL membranes clearly show that the level of asymmetry that is characteristic in the absence of CAP18 is reduced upon the addition of 110 nM CAP18 and the potential difference $\Delta\Phi$ rises from -35 to -30 mV. For the sake of clarification of the effect in Figure 4 A, the change of $\Delta\Phi$ from -35 to -7 mV after addition of 550 nM CAP18 is shown. Similar results were obtained for R595 LPS/PL membranes (data not shown).

On asymmetric bilayers made from R45 LPS from the resistant *P. mirabilis*, CAP18 induced completely opposite effects. The addition of 110 nM CAP18 led to a decrease in the potential difference $\Delta\Phi$ from -30 to -82 mV (Figure 4B).

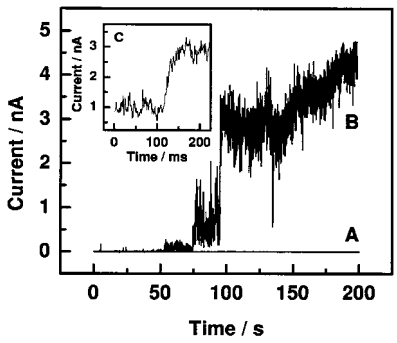

FIGURE 5: CAP18-induced current fluctuations. Macroscopic current trace in the absence (A) and presence (B) of CAP18 in the bathing solution. The inset (C) shows details of panel B at the moment of the current step 95 s after CAP18 addition (110 nM CAP18 added to the LPS side of a F515 LPS/PL bilayer at a clamp voltage of 40 mV). The bathing solution was 1000 mM KCl, 5 mM $MgCl_2$, and 5 mM HEPES at pH 7 and 37 °C.

In both cases, the effects were concentration-dependent. At higher concentrations, however, recording the *I*/*U* curves was not possible because of the induction of membrane lesions (see below).

Influence on Membrane Conductance. Membrane conductance is a measure of the integrity of the lipid bilayer. An intact, undisturbed solvent-free bilayer has a negligible electrical conductivity of <1 pA. Proteins and peptides may cause static or transient pores or lesions, leading to an increase in conductivity. Thus, the influence of CAP18 on membrane conductivity of differently composed lipid bilayers should yield information about the molecular interaction between the protein and the outer membrane of Gram-negative bacteria and, in particular, about the contribution of the membrane composition to resistance against CAP18. We have investigated three experimental parameters that describe the interaction between CAP18 and the differently composed bilayer: the minimal protein concentration c_{min} and the minimal clamp voltage V_{min} that is needed to induce membrane effects and the characteristics of the conductance changes, e.g., duration and amplitude.

First, we demonstrate the interaction of CAP18 with asymmetric F515 LPS/PL membranes as an example for the lipid matrix of a CAP18-sensitive strain. Effects on other lipid matrixes are described for comparison to obtain insight into the mechanisms underlying CAP18 resistance, to investigate lipid specificity, and to provide information for a model of the molecular interaction of CAP18 with the outer membrane.

The addition of CAP18 at a final concentration of about 110 nM, which is above the 50% inhibitory concentration of Gram-negative bacteria (*10*), to the LPS side of an asymmetric F515 LPS/PL planar bilayer membrane at a clamp voltage of 20 mV (PL side grounded), led to a noise-like increase in membrane current characterized by transient current fluctuations (Figure 5B,C), indicating the induction of transient membrane lesions. The amplitudes of the current fluctuations (Figure 6) and their lifetimes were determined by a visual inspection of the current traces. From the mean current *I* of the single fluctuations at a clamp voltage *U* in a bathing solution with a specific conductivity σ, the mean diameter *d* of the respective membrane lesion could be calculated according to the simple relation $I = (\pi\sigma d^2 U)/(4l)$

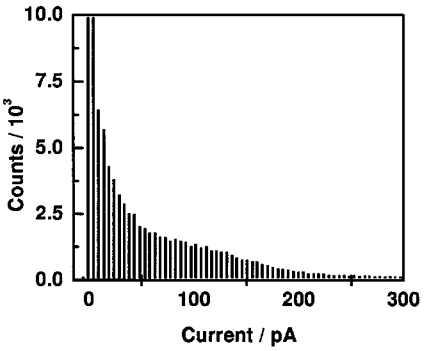

FIGURE 6: Distribution of the amplitudes of the current fluctuations induced by the addition of CAP18 to the bilayer. Same expermiment whose results are depicted in Figure 5 (220 nM CAP18 added to the LPS side of a F515 LPS/PL bilayer at a clamp voltage of 40 mV) in the time interval from the beginning to 90 s. The bathing solution was 1000 mM KCl, 5 mM $MgCl_2$, and 5 mM HEPES at pH 7 and 37 °C.

(*16*). For this, a circular geometry of the lesion and a membrane thickness l of 6 nm were assumed.

The leasion diameters had no discrete values but a broad distribution from below 0.2 ± 0.1 nm in the initial phase (Figures 5B, 6, and 7) up to more than 5.0 ± 1 nm (Figure 5C). Also, the lifetimes of the current fluctuations were not uniformly distributed. Most of the smaller lesions had a lifetime of <2 ms, but large lesions with lifetimes on the order of minutes were also observed (Figure 5B from 100 s on).

To investigate the influence of the transmembrane potential on the formation and characteristics of CAP18-induced membrane lesions, a triangular voltage with an amplitude of ±80 mV was applied (Figure 8A). In all bilayers that were investigated, CAP18 induced current fluctuations at a lipid-specific positive clamp voltage as it can be seen in sections 1 and 3 of Figure 8B. During the first negative voltage cycle (Figure 8B, section 2), in some experiments some small fluctuations could be observed which did not appear after a complete negative and positive cycle (Figure 8B, section 4). Also when starting with a negative voltage cycle, we obtained the same results. This behavior was found for F515 LPS/PL as well as for R45 LPS/PL membranes.

Membranes become very unstable after addition of CAP18, and this causes membrane rupture especially at clamp voltages above 80 mV.

Different salt concentrations in the subphase (e.g., a KCl concentration of up to 1 M; see Figures 5 and 7A) or reduction of the $MgCl_2$ concentration from 5 to 0 mM did not change the characteristics of the lesions (data not shown).

The lipid specificity of CAP18 may thus be summarized as follows. CAP18 induces lesions in F515 LPS/PL, R595 LPS/PL, R45 LPS/PL, PL/PL, and even DPhyPC/PL membranes. No correlation between the minimal concentration c_{min} needed for the induction of the lesions at the same clamp voltage and the lipid matrix was observed. However, there was a dependence of c_{min} on the minimal clamp voltage (V_{min}). The CAP18 concentration needed to induce lesions was lower at higher clamp voltages.

Furthermore, we did not observe any differences in the microscopic characteristics of the lesions in the different bilayers. In Figure 7, current traces of different membranes and at different salt concentrations are shown in the initial phase after CAP18 addition. For a better comparison, the current is normalized to the specific conductance, and the applied clamp voltage, i.e., the size parameter $I/(U\sigma)$, is depicted instead of membrane current.

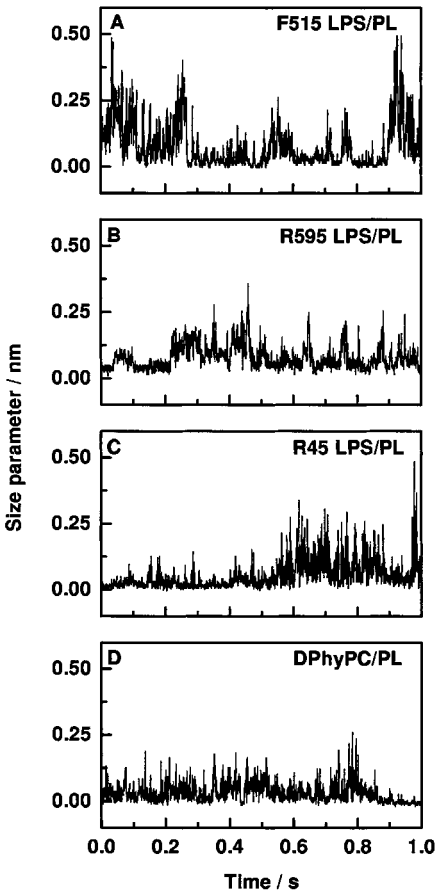

FIGURE 7: Size parameter $I/(U\sigma)$ of current fluctuations vs time in the initial phase after the addition of CAP18 in differently composed membranes (the side of CAP18 addition is named first): (A) F515 LPS/PL, 110 nM CAP18, U = 40 mV, bathing solution of 1000 mM KCl, 5 mM $MgCl_2$, and 5 mM HEPES at pH 7 and 37 °C (initial phase taken from Figure 5); (B) R595 LPS/PL, 55 nM CAP18, U = 60 mV, bathing solution of 100 mM KCl, 5 mM $MgCl_2$, and 5 mM HEPES at pH 7 and 37 °C; (C) R45 LPS/PL, 110 nM CAP18, U = 80 mV, bathing solution of 100 mM KCl, 5 mM $MgCl_2$, and 5 mM HEPES at pH 7 and 37 °C; and (D) DPhyPC/PL, 55 nM CAP18, U = 60 mV, bathing solution of 100 mM KCl, 5 mM $MgCl_2$, and 5 mM HEPES at pH 7 and 37 °C.

In contrast to these similarities, the V_{min} required for the induction of current fluctuations after the addition of 110 nM CAP18 was significantly different for the various membrane systems. This can easily be deduced from the I/U curves of the respective membrane systems (Figure 9). V_{min} increased in the following order: F515 LPS/PL (Figure 9B) and R595 LPS/PL < R45 LPS/PL (Figure 9A) < DPhyPC/PL bilayers (Table 1). With a 10-fold higher amount of CAP18, however, for R45 LPS/PL bilayers the V_{min} was also reduced to 20 ± 10 mV, a value comparable to that observed for F515 LPS/PL membranes at a CAP18 concentration of 110 nM. Comparable results were obtained with subphases in the absence of $MgCl_2$.

Inhibition of CAP18 by Heparin. To show that heparin not only inhibited the LPS-neutralizing activity of CAP18 as shown by Ogata et al. (*7*) but also inhibits the antibacterial activity, we determined the capacitance of F515 LPS/PL

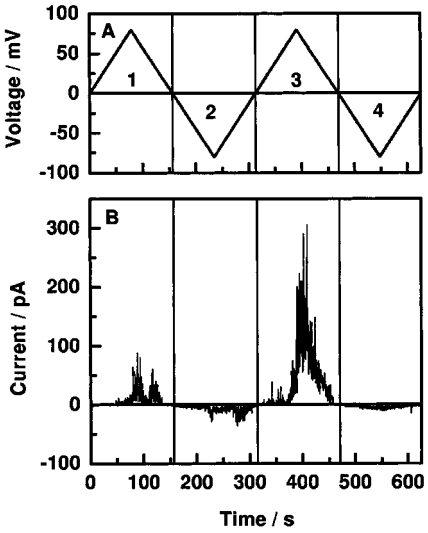

FIGURE 8: Current fluctuations and clamp voltage vs time. Addition of 110 nM CAP18 to the LPS side of F515 LPS/PL bilayer: (A) clamp voltage trace and (B) current trace. The bathing solution was 100 mM KCl, 5 mM $MgCl_2$, and 5 mM HEPES at pH 7 and 37 °C.

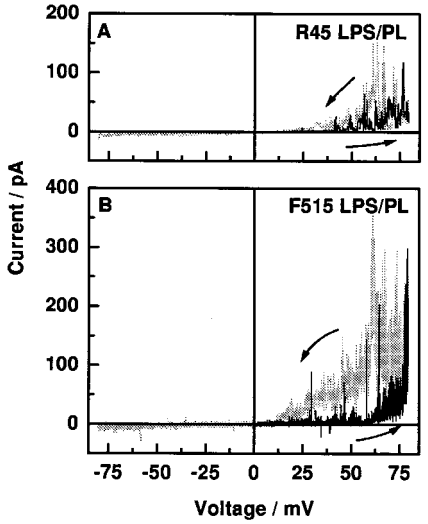

FIGURE 9: Voltage dependence of current fluctuations. *I*/*U* curves for asymmetric bilayers after the addition of 110 nM CAP18 to the LPS side of a (A) R45 LPS/PL bilayer or (B) F515 LPS/PL bilayer. The bathing solution was 100 mM KCl, 5 mM $MgCl_2$, and 5 mM HEPES at pH 7 and 37 °C: (arrows to the right and black traces) clamp voltage ramp from 0 up to 80 mV and (arrows to the left and gray traces) clamp voltage ramp from 80 down to −80 mV.

membranes before and after addition of 55 nM CAP18 preincubated with ≈30 nM heparin. In the experiment whose results are depicted in Figure 10, we first added ≈60 nM heparin to the F515 LPS side of the bilayer, to demonstrate that there is no interaction between heparin itself and the membrane. Also, the addition of the preincubated CAP18/heparin did not induce capacitance changes. Only the addition of a large molar excess (1 μM) of CAP18 led to the typical increase in capacitance and a final membrane rupture.

DISCUSSION

CAP18 and its bioactive C-terminal fragments are bactericidal against a variety of Gram-neagtive bacteria, although there are exceptions such as *P. mirabilis*. Previous studies

Table 1: Molecular Parameters of Lipids and Results of Planar Membrane Experiments[a]

(glyco)lipid	molecular charge[b] e_0	charge density[b] e_0/nm^2	relative change of C_M	relative change of $\lvert\Delta\Phi\rvert$	V_{min} (mV)
F515 LPS	−4	−3.1	++	decrease	10 ± 4
R595 LPS	−3.4	−2.4	++	decrease	10 ± 5
R45 LPS	−3	−2.0	+	increase	30 ± 5
DPhyPC	0	0	none	none	60 ± 7

[a] Molecular parameters describing the (glyco)lipids composing the bilayer leaflet at the side of CAP18 addition of various asymmetric planar bilyers (the second leaflet was always made from the phospholipid mixture), change in membrane capacitance C_M, and innermembrane potential difference $\Delta\Phi$ after CAP18 addition and the avarage minimal clamp voltage V_{min} needed to induce membrane lesions. [b] Taken from ref *17*.

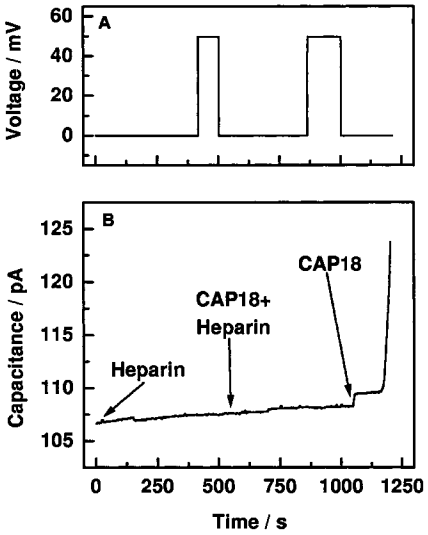

FIGURE 10: Inhibition of CAP18 by heparin. Clamp voltage (trace A) and capacitance (trace B) vs time for an asymmetric F515 LPS/PL bilayer. Additions of 60 nM heparin (t = 0 s), 55 nM CAP18 preincubated with 30 nM heparin (t = 550 s), and 1.1 μM CAP18 (t = 1050 s) are denoted by arrows. The bathing solution was 100 mM KCl, 5 mM $MgCl_2$, and 5 mM HEPES at pH 7 and 37 °C.

showed that polycationic CAP18 peptides bind to negatively charged lipids, although the cationic nature of the peptides is not the sole determinant required for membrane-permeabilizing activity (*10*). Apparently, the α-helical conformation and amphipathicity of the peptides are also important factors in the interaction with the bacterial cell wall (*9*).

Mason et al. (*11*) discussed that the $CAP18_{106-137}$-induced membrane permeabilization is the primary killing event. Our TEM pictures (Figure 2) clearly show that CAP18 destroyed the integrity of the outer membrane of the organisms of the CAP18-sensitive *E. coli* strains. Compared to the deep rough mutant *E. coli* F515 strain, even the longer sugar moiety of the wild-type *E. coli* ATCC 11775 strain does not protect the bacteria against the bactericidal activity of CAP18. In contrast to this observation, the outer membrane of the CAP18-resistant *P. mirabilis* remained intact. The CAP18 concentration (110 nM) used in the experiments whose results are depicted in Figure 1 is higher than the 50% inhibitory concentration, and thus, the observed damage might have progressed further, possibly beyond the frequently observed membrane blebbing [e.g., for human defensins (*25*)]. Although these results do not verify that the perme-

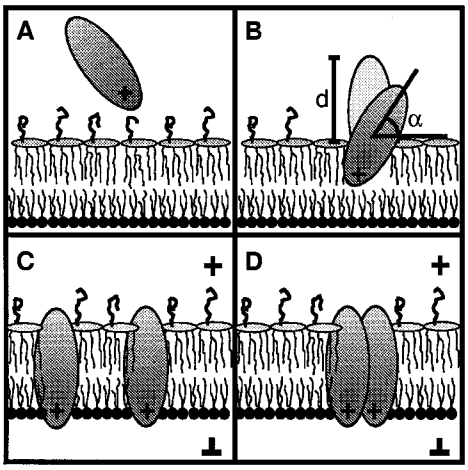

FIGURE 11: Model for the interaction between rabbit CAP18 and LPS/PL bilayers: (A) accumulation of CAP18 at the membrane surface (aqueous state), (B) intercalation of the protein into the membrane (nonconductive state) [differently deep intercalation (*d*) or orientation (α) in diffentely composed LPS/PL bilayers is indicated by two protein molecules], (C) change in protein orientation into a transmembrane configuration (nonconductive state), and (D) formation of transient lesions by aggregation (conductive state).

abilization of the outer membrane is the sole event leading to cell death, they support the conclusion that it is a primary and necessary event for killing the bacteria as it is the case for OM permeabilization by polymyxin B where outer membrane passage, i.e., the "self-promoted" uptake, is the initial event in bacterial killing (*17*, *26*). However, it is likely that differences in the compositions of the outer membrane of Gram-negative bacteria contribute to bacterial sensitivity or resistance to CAP18.

To gain more insight into the mechanisms underlying the antibacterial activity of CAP18 and to investigate the influence of the lipid matrix on sensitivity, we studied the interaction of rabbit CAP18 with various reconstituted planar membranes, including asymmetric bilayers composed of different LPS on one side and a phospholipid mixture on the other as a model of the outer membrane of Gram-negative bacteria.

According to our data, we can set up a model for the interaction between rabbit CAP18 and LPS/PL bilayers which consists of five steps (Figure 11): (1) accumulation of CAP18 at the membrane surface (aqueous state), (2) intercalation of the protein into the membrane (nonconductive surface state), (3) change of the orientation of the protein by a positive clamp voltage (also required in step 4) (nonconductive prelesion state), (4) formation of transient lesions (conductive state), and (5) closing of the lesions (nonconductive postlesion state) (Figure 11).

CAP18 is drawn as an oval molecule in Figure 11 largely because the secondary structure of the protein is not yet known in detail. Nevertheless, it is obvious that the α-helical C-terminal domain has an exposed positively charged structure (*5*, *8*).

In the following, we will discuss the various types of experimental evidence for this model and the involved steps.

(1) The accumulation of the polycationic CAP18, which carries 11 net positive charges (by calculation), at the negatively charged LPS surface of LPS/PL membranes is the first and prerequisite step (Figure 11A). The influence of the accumulation on the interaction process is not as pronounced as in the case of polymyxin B (PMB) (*17*), on the basis of the following observations. A reduction in the number of positive charges in fragments of $CAP18_{106-125}$ has a smaller effect on the activity than the change in its α-helical conformation or amphipathicity (*9*). The lack of Mg^{2+} dependence in the concentration range of 0−10 mM further confirms that the electrostatic interaction between CAP18 and the membrane is not the sole important step in the interaction. To further verify this statement, we are at present investigating the $^{45}Ca^{2+}$-displacing capacity of CAP18 from LPS monolayers and the influence of divalent cations on the intercalation of CAP18 into LPS monolayers using the Langmuir technique.

Moreover, we could not find significant differences in minimal CAP18 concentrations (c_{min} = 50−500 nM) required to induce the formation of lesions in lipid matrixes with different surface charge densities if the minimal clamp voltage (Table 1) was high enough for the induction of lesions. To produce the same effect at an identical clamp voltage, a higher CAP18 concentration was needed for R45 LPS/PL membranes than for F515 LPS/PL and R595 LPS/PL membranes.

For the PMB-induced lesions, the minimal peptide concentration varied in a range between 1 and 50 μM which correlates with the charge density of the bilayer leaflet facing the side of addition (*17*). Such a simple correlation could not be found for the interaction between CAP18 and lipid bilayers, because c_{min} varied in a smaller range and depended on the applied clamp voltage.

(2) As can be seen from the results of the capacitance and innermembrane potential measurements, the composition of the outer leaflet in terms of the existence of negative surface charges is important for the intercalation of rabbit CAP18 into bilayers.

A change in membrane capacitance could be observed only for membranes consisting of a negatively charged leaflet on the side of CAP18 addition. Furthermore, the effects were reduced in the case of R45 LPS/PL in contrast to F515 LPS/PL or R595 LPS/PL membranes (Figure 3) which could by due to a lower amount of intercalated CAP18 or to a different orientation of the protein in the bilayers. It is known that the 4′-phosphate of the lipid A of the CAP18-sensitive *S. minnesota* and the first Kdo of the LPS of the CAP18-resistant *P. mirabilis* are substituted with cationic L-Ara*p*4N (*27*). The reduction in the molecular net charge from F515 LPS (e_0 = −4) and R595 LPS (e_0 = −3.4) to R45 LPS (e_0 = −3) could explain a lower binding stoichiometry between the R45 LPS and CAP18. We have, however, observed nearly the same change in capacitance for F515 LPS/PL and R595 LPS/PL membranes and a strongly reduced change for R45 LPS/PL membranes. From these results, we propose that the L-Ara*p*4N at the Kdo of the LPS of *P. mirabilis* leads to steric hindrance resulting in a different orientation of the CAP18 protein in the bilayer.

To support this hypothesis, we investigated the influence of rabbit CAP18 on the innermembrane potential difference (ΔΦ) and found that ΔΦ increased from −35 mV to higher values in a concentration-dependent manner after the addition of CAP18 to F515 LPS/PL and R595 LPS/PL membranes, whereas ΔΦ decreased from −30 mV to lower values in the case of R45 LPS/PL membranes (Figure 4). Obviously,

these different effects cannot be explained by the amount of intercalated CAP18. The different effects on $\Delta\Phi$ rather suggest two different possibilities of interaction. (i) CAP18 reduces the negative Gouy−Chapman potential of all three LPS/PL membranes, similar to the effects of Mg^{2+} and PMBN (*28*). In the case of F515 LPS/PL and R595 LPS/PL membranes, a reduction of the positive dipole potential also occurs, leading to an increase in $\Delta\Phi$. (ii) CAP18 increases the dipole potential, but only in the case of F515 LPS/PL and R595/PL membranes is the dipole potential of the PL leaflet also increased. This would then lead to a reduction in $\Delta\Phi$.

Both assumptions have in common the fact that rabbit CAP18 intercalates deeper into the membrane of sensitive bacteria than into that of the CAP18-resistant *P. mirabilis*.

In Figure 11B, we illustrate that the difference in the orientation of the protein could refer to either a different depth of integration *d* or a different angle α betweeen the protein and the membrane surface. In our experiments, we could not distinguish between these two possibilities.

(3 and 4) For the induction of lesions, a lipid-specific positive clamp voltage V_{min} was required in all the membrane systems that were studied (Figure 9 and Table 1). V_{min} was lowest for those membrane systems with the highest degree of intercalation of CAP18. In Gram-negative bacteria, the periplasmic space is strongly anionic as compared to the external medium, which is mainly caused by the anionic membrane-derived oligosaccharides (MDO) (*29*). MDO contribute to the Donnan potential across the outer membrane which was determined for *E. coli* in the presence of an external cation concentration of 100 mM to be 26 mV (inside negative) (*30*). This value is in good agreement with our observation that V_{min} for asymmetric bilayers, repesenting the lipid matrix of the CAP18-sensitive bacteria (F515 LPS/PL and R595 LPS/PL membranes), is lower and that for R45 LPS/PL membranes, repesenting the lipid matrix of the resistant strain *P. mirabilis* R45, is higher than this value.

Cafiso (*31*) proposed four different models for the voltage-dependent gating of the antibiotic alamethicin: (a) voltage-dependent structural change of the peptide molecules, (b) voltage-dependent dipole reorientation, (c) voltage-dependent partitioning, and (d) voltage-dependent insertion into the lipid matrix.

From the observation that CAP18 can permeabilize neutral/zwitterionic DPhyPC/PL membrane at clamp voltages above 60 mV (Figure 7B), the assumption of a voltage-dependent partitioning mechanism is resonable, because no intercalation of the protein could be observed at zero clamp voltages. In the case of bilayers consisting of a negatively charged leaflet on the side of protein addition, an intercalation and/or partitioning took place at a clamp voltage of 0 mV. Thus, a voltage-dependent partitioning of the protein into the membrane was not essential anymore, and a voltage-dependent insertion was likely.

In the model described by Baumann and Mueller (*32*) for the interaction of alamethicin with planar bilayers, a voltage-dependent change in the orientation of the peptide, from a surface to a transmembrane orientation, leads to its gating.

Depending on the different initial orientation and/or position of CAP18 in the lipid bilayer, different positive clamp voltages are required to transfer the molecules into a transmembrane orientation. The conductive state at negative voltages, which could be observed at the initial application of a negative clamp voltage (Figure 8B), might be explained by an incomplete "correct" orientation of the molecules.

On the basis of this more complex initial state, we have extended the alamethicin model to explain the action of CAP18. CAP18 intercalates into bilayers in a lipid-specific orientation which could be changed by positive clamp voltages. The amplitude of the required voltage is inversely proportional to the degree of intercalation and forces the protein into a transmembrane configuration (Figure 11C). Higher protein concentrations may reduce V_{min}, because larger numbers of CAP18 molecules are in the correct transmembrane orientation. A direct correlation between the peptide-to-lipid ratios at the membrane and V_{min} could not be given, because in the experimental setup, further lipid layers on the surface of the subphase and possibly on the walls of the compartments exist besides the bilayer membrane that is being investigated. Thus, the effective lipid concentration that is accessible for protein interaction cannot be determined.

From our data, a confirmation of the model of Matsuzaki et al. (*33*), who proposed that α-helical antimicrobial peptides are complexed with lipids which they transport into the inner leaflet of the membrane during the flipping process, is not possible.

The concentration dependence of the conductivity is most easily interpreted in terms of a multimeric channel structure, which seems reasonable considering the amphipathic nature of the protein. Furthermore, the diameters and lifetimes of the CAP18-induced lesions are very heterogeneous (Figure 6), indicating that the lesions are formed by aggregates of a varying number of molecules. Therefore, the multipore cluster model is more suitable for an explanation of the observed effects than the barrel-stave model which was proposed for the alamethicin channel which exhibits multi-step conductances (*31*).

We postulate that the current fluctuations are not caused by well-defined channels, but rather by lesions or defects in the bilayer formed by CAP18 oligo- or multimers. Johansson et al. (*34*) showed that LL-37 (human $CAP18_{104-140}$) requires such an oligomeric conformation for optimal antibacterial activity. The formation of CAP18 membrane lesions is shown in part D of our model. A number of CAP18 molecules are forced into a transmembrane configuration by a postive clamp voltage. Lateral diffusion of the protein molecules in the membrane leads to their aggregation and the formation of a so-called multipore cluster (*31*) with heterogeneous diameters (Figures 5B,C and 6). At low numbers, the lesions destabilize the planar membranes, and at higher numbers, they disrupt their functional integrity. For the bacterial organism, this implies that CAP18 after having distroyed the permeation barrier of the outer membrane could induce lethal leakages in the cytoplasmic membrane.

We suspect the composition of the negative lipid matrix plays only a minor role in the formation of the lesions, because we could not detect a lipid specificity (Figure 7) of the characteristics of the lesion.

(5) The limited lifetimes of the lesions at a clamp voltage above V_{min} may be explained by the instabilites of the bilayer defects and the lateral diffusion of the CAP18 molecules in the membrane caused by concentration gradients and leading to a decrease in the local CAP18 concentration below the

critical value of protein aggregation (Figure 11C) as a prerequisite for the conductive state. A second possible mechanism for explaining the closing of the lesions could be a change in the orientation of CAP18 from a transmembrane to a surface-orientated state on the PL side of the membranes.

At a clamp voltage below V_{min}, the CAP18 molecules reorientated from the transmembrane configuration into the surface-orientated state, and the formation of lesions was inhibited (Figure 8B).

The C-terminal domain of CAP18 which is responsible for the LPS-binding and LPS-neutralizing activities is also a target for the binding of heparin and inhibits the activities of CAP18 (*6*, *7*). Our data include an explanation of the capacity of heparin to inhibit the permeabilization of the outer membrane by CAP18 (Figure 10), because the intercalation into the membrane is already inhibited. Thus, the mechanism of interaction of the polycationic CAP18 with the negatively charged membrane is already blocked in the first or second step of our model (Figure 11A,B). Whether the accumulation of CAP18 at the membrane or the intercalation into the membrane is inhibited by heparin cannot be answered by our experiments. From the structure of heparin, both explanations are possible, because on one hand the anionic heparin neutralizes some or all postive charges of CAP18 and on the other hand the CAP18−heparin complex might have a geometry and properties making an intercalation impossible.

In summary, our data show that the permeabilization of the outer membrane of Gram-negative bacteria by rabbit CAP18 is the primary and a necessary event in the killing process of bacteria.

The accumulation at and intercalation into the membrane are mediated by electrostatic interactions of the polycationic protein with the negatively charged LPS surface. The depth of intercalation and/or the orientation of the proteins depends on other factors such as sterical hindrance. It is likely that the different degree of intercalation correlating with the minimal clamp voltage needed to induce transient lesions and membrane rupture is the reason for resistance or sensitivity. Furthermore, the intercalation of CAP18 leads to different changes in the transmembrane potential, thereby influencing the gating behavior of outer membrane proteins. These effects can be explained by our five-step model.

It has been proposed that the antibacterial target of cationic peptides and proteins is the cytoplasmic membrane (*35*). It is possible that CAP18 permeates the outer membrane after formation of lesions by the self-promoted uptake and enters the cytoplasmic space. The observation that CAP18 also induces lesions in PL/PL and DPhyPC/PL membranes at a clamp voltage above 60 mV (outside postive), which is much lower than the potential gradient of about −150 mV (inside negative) across the cytoplasmic membrane (*36*), clearly shows that CAP18 could permeate the inner membrane, thus allowing ions to equilibrate across the cytoplasmic membrane to reduce or destroy the membrane potential. Wu et al. (*37*) showed this for some cationic peptides, but they also pointed out that there was no absolute correlation between the ability to permeabilize the cytoplasmic membrane and the antimicrobial activity. This leaves the possibility open that the actual targets for these cationic peptides are located in the cytoplasm.

Further details are the subject of investigations with different biophysical techniques and different CAP18 fragments (paper in preparation).

ACKNOWLEDGMENT

We thank Mrs. Heike Kühl for preparing the electron micrographs.

REFERENCES

1. Cowland, J. B., Johsen, A. H., and Borregaard, N. (1995) *FEBS Lett. 368*, 173−176.
2. Larrick, J. W., Morgan, J. G., Palings, I., Hirata, M., and Yen, M. H. (1991) *Biochem. Biophys. Res. Commun. 179*, 170−175.
3. Sørensen, O., Cowland, J. B., Askaa, J., and Borregaard, N. (1997) *J. Immunol. Methods 206*, 53−59.
4. Hirata, M., Zhong, J., Wright, S. C., and Larrick, J. W. (1995) *Prog. Clin. Biol. Res. 392*, 317−326.
5. Larrick, J. W., Hirata, M., Zheng, H., Zhong, J., Bolin, D., Cavaillon, J.-M., Shaw Warren, H., and Wright, S. C. (1994) *J. Immunol. 152*, 231−240.
6. Hirata, M., Shimomura, Y., Yoshida, M., Wright, S. C., and Larrick, J. W. (1994*) Prog. Clin. Biol. Res. 388*, 147−159.
7. Ogata, M., Fletcher, M. F., Kloczewiak, M., Loiselle, P. M., Zanzot, E. M., Vermeulen, M. W., and Shaw Warren, H. (1997) *Infect. Immun. 65*, 2160−2167.
8. Chen, C., Brock, R., Luh, F., Chou, P.-J., Larrick, J. W., Huang, R.-F., and Huang, T.-H. (1995) *FEBS Lett. 370*, 46−52.
9. Tossi, A., Scocchi, M., Skerlavaj, B., and Gennaro, R. (1994) *FEBS Lett. 339*, 108−112.
10. Larrick, J. W., Hirata, M., Shimomoura, Y., Yoshida, M., Zheng, H., Zhong, J., and Wright, S. C. (1993) *Antimicrob. Agents Chemother. 37*, 2534−2539.
11. Mason, D. J., Dybowski, R., Larrick, J. W., and Gant, V. A. (1997) *Antimicrob. Agents Chemother. 41*, 624−629.
12. Rietschel, E. T., Kirikae, T., Schade, F. U., Mamat, U., Schmidt, G., Loppnow, H., Ulmer, A. J., Zähringer, U., Seydel, U., Di Padova, F., Schreier, M., and Brade, H. (1994) *FASEB J. 8*, 217−225.
13. Montal, M., and Mueller, P. (1972) *Proc. Natl. Acad. Sci. U.S.A. 69*, 3561−3566.
14. Zähringer, U., Lindner, B., Seydel, U., Rietschel, E. T., Naoki, H., Unger, F. M., Imoto, M., Kusumoto, S., and Shiba, T. (1985) *Tetrahedron Lett. 26*, 6321−6324.
15. Rietschel, E. T., Brade, L., Lindner, B., and Zähringer, U. (1992) in *Bacterial endotoxic lipopolysaccharides, Vol. I: Molecular biochemestry and cellular biology* (Morrison, D. C., and Ryan, J. L., Eds.) pp 3−41, CRC Press, Boca Raton, FL.
16. Vinogradov, E. V., Thomas-Oates, J. E., Brade, H., and Holst, O. (1994) *J. Endotoxin Res. 1*, 199−206.
17. Wiese, A., Münstermann, M., Gutsmann, T., Lindner, B., Kawahara, K., Zähringer, U., and Seydel, U. (1998) *J. Membr. Biol. 162*, 127−138.
18. Galanos, C., Lüderitz, O., and Westphal, O. (1969) *Eur. J. Biochem. 9*, 245−249.
19. Seydel, U., Schröder, G., and Brandenburg, K. (1989) *J. Membr. Biol. 109*, 95−103.
20. Osborn, M. J., Gander, J. E., Parisi, E., and Carson, J. (1972) *J. Biol. Chem. 247*, 3962−3972.
21. Shaw, N. (1974) *Adv. Appl. Microbiol. 17*, 63−108.
22. Alvarez, O., and Latorre, R. (1978) *Biophys. J. 21*, 1−17.
23. Schoch, P., Sargent, D. F., and Schwyzer, R. (1979) *J. Membr. Biol. 46*, 71−89.
24. Seydel, U., Eberstein, W., Schröder, G., and Brandenburg, K. (1992) *Z. Naturforsch. 47c*, 757−761.
25. Lehrer, R. I., Barton, A., Daher, K. A., Harwig, S. S. L., Ganz, T., and Selsted, M. E. (1989) *J. Clin. Invest. 84*, 553−561.
26. Hancock, R. E. W. (1984) *Annu. Rev. Microbiol. 38*, 237−264.

27. Kaca, W., Radziejewska-Lebrecht, J., and Bhat, U. R. (1990) *Microbios 61*, 23−32.
28. Wiese, A., Brandenburg, K., Carroll, S. F., Rietschel, E. T., and Seydel, U. (1997) *Biochemistry 36*, 10311−10319.
29. Benz, R. (1994) in *Bacterial Cell Wall* (Ghuysen, J.-M., and Hakenbeck, R., Eds.) pp 397−423, Elsevier Science B. V., Amsterdam.
30. Sen, K., Hellman, J., and Nikaido, H. (1988) *J. Biol. Chem. 25*, 1182−1187.
31. Cafiso, D. S. (1994) *Annu. Rev. Biophys. Biomol. Struct. 23*, 141−165.
32. Baumann, G., and Mueller, P. (1974) *J. Supramol. Struct. 2*, 538−557.
33. Matsuzaki, K., Mitani, Y., Akada, K. Y., Murase, O., Yoneyama, S., Zasloff, M., and Miyajima, K. (1998) *Biochemistry 37*, 15144−15153.
34. Johansson, J., Gudmundsson, G. H., Rottenberg, M. E., Berndt, K. D., and Agerberth, B. (1998) *J. Biol. Chem. 273*, 3718−3724.
35. Duclohier, H., Molle, G., and Spach, G. (1989) *Biophys. J. 56*, 1017−1023.
36. Bakker, E. P., and Mangerich, W. E. (1981) *J. Bacteriol. 147*, 820−826.
37. Wu, M., Maier, E., Benz, R., and Hancock, R. E. W. (1999) *Biochemistry 38*, 7235−7242.

BI990643V